Brain palpation from physiological vibrations using MRI

Ali Zorgani[a,b], Rémi Souchon[a,b], Au-Hoang Dinh[a,b], Jean-Yves Chapelon[a,b], Jean-Michel Ménager[c], Samir Lounis[c], Olivier Rouvière[a,b,d], and Stefan Catheline[a,b,1]

[a]Inserm, U1032, LabTau, Lyon, F-69003, France; [b]Université Lyon 1, Lyon, F-69003, France; [c]Centre Radiologie Imagerie par Résonance Magnétique (IRM) Préssensé, Villeurbanne, F-69100, France; and [d]Hospices Civils de Lyon, Hôpital Edouard Herriot, Lyon, F-69003, France

Edited by David A. Weitz, Harvard University, Cambridge, MA, and approved September 1, 2015 (received for review May 21, 2015)

We present a magnetic resonance elastography approach for tissue characterization that is inspired by seismic noise correlation and time reversal. The idea consists of extracting the elasticity from the natural shear waves in living tissues that are caused by cardiac motion, blood pulsatility, and any muscle activity. In contrast to other magnetic resonance elastography techniques, this noise-based approach is, thus, passive and broadband and does not need any synchronization with sources. The experimental demonstration is conducted in a calibrated phantom and in vivo in the brain of two healthy volunteers. Potential applications of this "brain palpation" approach for characterizing brain anomalies and diseases are foreseen.

elastography | brain | correlation

The complexity of wave fields can sometimes be an advantage for imaging. Such is the case in multiple scattering or reverberating media, where wave fields contain information about their sources and the medium itself. Turning this wave noise into useful measurements through correlation techniques has provided a breakthrough in a wide variety of domains, which range from seismology (1) to acoustics (2, 3) and electromagnetism (4). Living tissue is also full of unexploited vibrations. Their detection with ultrafast ultrasound scanners that can reach thousands of frames per second (5–7) has recently opened up the medical field to correlation techniques and therefore, passive elastography (8). However, ultrasound is not suitable for brain imaging. MRI can image the brain, but its relatively low acquisition rate of a few frames per second is an issue. Synchronization with the shear-wave source is, thus, necessary (9, 10), which penalizes its potential implementation based on natural shear waves.

We describe a magnetic resonance elastography (MRE) -based method that is free from the need for synchronization and any controlled source. This approach extracts information related to the mechanical properties of the soft tissue from hundreds of snapshots of randomly fluctuating shear-wave fields. The key to decrypting the complex field is correlation or similarly but from a physical point of view, time reversal (11, 12). Not only does this wide-band approach maximize the signal-to-noise ratio, as any matched filter would, but it also avoids the Nyquist–Shannon problem that is inherent to slow imaging devices. Indeed, although time information is definitely lost, the spatial information is still present and allows shear-wavelength tomography to be conducted. This wavelength is closely related to the shear elasticity and thus, the intuitive estimation of the stiffness felt by physicians during palpation examination. To start, this concept is shown using MRI in a calibrated elastography phantom under randomly sampled vibrations. Arterial pulsation can produce motion in the brain as high as 1 mm (13); the resulting natural shear-wave field is analyzed through correlation algorithms, and passive brain palpation reconstructions are presented.

Results

Phantom Experiments. As shown in the experimental setup (Fig. 1*A*), vibrations are generated synchronously from 12 contact points of a device mounted on a piezoelectric source and working with a 80.3-s modulated sinusoid excitation. The emitted frequencies range from 20 to 200 Hz. These vibrations propagate mainly as shear waves within a phantom designed for elastography tests (Computerized Imaging Reference Systems, Inc.) that contains four calibrated inclusions. The emitted waves reverberate inside this soft, solid cavity, and the resulting complex field is measured every 1.5 s using an MRI scanner. It is important to point out first that the vibrations driving are continuously repeated during the whole acquisition time and second, that the modulated sinusoid duration of 80.3 s divided by the imaging frame rate of 1.5 s is not an integer to avoid any cyclic sampling of the field. Each frame contains 128 × 128 pixels. The acquisition of 320 frames for the out-of-plane component of the displacement field was carried out at ∼0.7 Hz on six slices that were equally spaced by 3 mm, with $3 \times 3 \times 3\text{-mm}^3$ isotropic voxels, over 8 min. According to the Nyquist–Shannon limit, the maximum shear-wave frequency was, thus, ∼0.35 Hz, which is far below the central frequency of shear waves in the experiment. The first six consecutive snapshots of the displacement field of a total of 320 snapshots are shown in Fig. 1*B*. These snapshots clearly show the rectangular phantom surrounded by the random-phase noise. The elastic field shows complex spatial patterns with characteristic dimensions driven by the wavelengths associated with the 20- to 200-Hz frequency content of the sweep source signal. Small wavelengths are visible at $t = 1.5$ s, whereas larger wavelengths dominate at $t = 3$ s. A correlation coefficient smaller than 5% between consecutive snapshots of wave pattern confirms the random property of the diffuse elastic field. The extraction of the elastic parameters from 320 snapshots was then carried out using noise correlation.

Theory. Let $\varphi_i(\vec{r},t)$ be the experimental observation of the i component of an elastic wave field $i = 1, 2, 3$. Then, a time convolution

Significance

It is commonly supposed that noise obscures but does not contain useful information. However, in wave physics and especially, seismology, scientists developed some tools known as "noise correlation" to extract useful information and construct images from the random vibrations of a medium. Living tissues are full of unexploited vibrations as well. In this manuscript, we show that noise correlation techniques in the brain using MRI can conduct to a tomography related to the stiffness that physicians estimate during a palpation examination. This MRI brain seismology in rupture with other techniques is experimentally shown in vitro and in vivo.

Author contributions: R.S., J.-Y.C., and S.C. designed research; A.Z., R.S., A.-H.D., S.L., and S.C. performed research; J.-M.M. and O.R. analyzed data; and A.Z. and S.C. wrote the paper.

The authors declare no conflict of interest.

This article is a PNAS Direct Submission.

[1]To whom correspondence should be addressed. Email: stefan.catheline@inserm.fr.

This article contains supporting information online at www.pnas.org/lookup/suppl/doi:10.1073/pnas.1509895112/-/DCSupplemental.

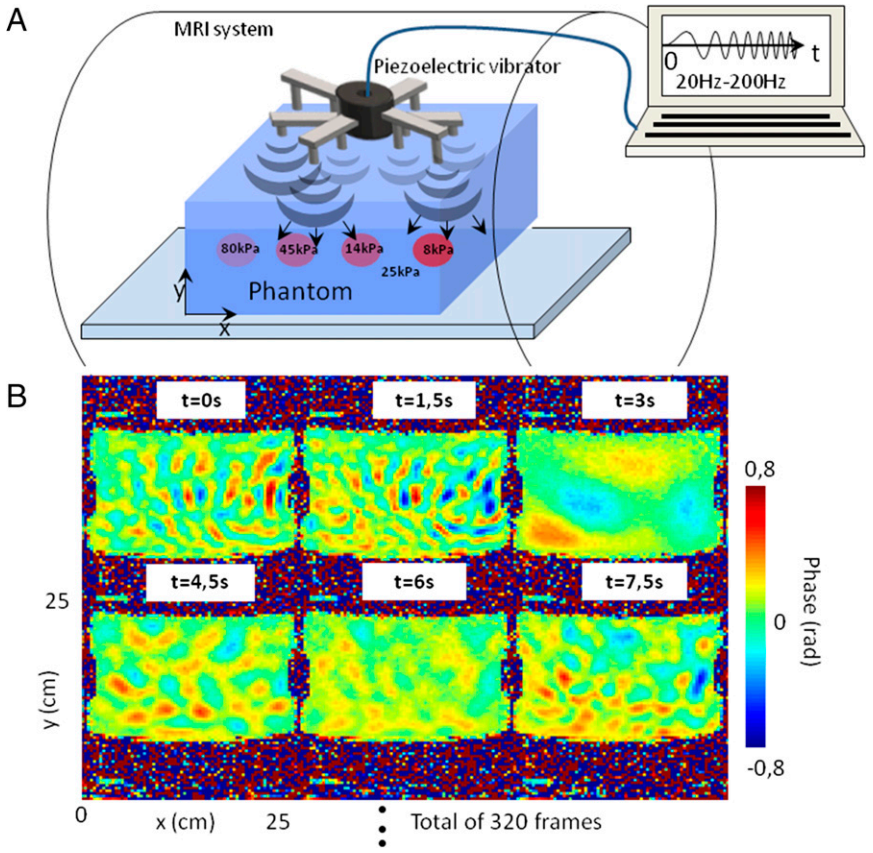

Fig. 1. (*A*) Experimental setup. The complex shear-wave field is generated from 12 point sources located at the surface and mounted on an MRI-compatible piezoelectric vibrator. The excitation signal is an 80.3-s modulated sinusoid, with the frequency range of 20 to 200 Hz. (*B*) Phase images that represent the out-of-plane displacement field u_y in the *zx* plane of the inclusions. These first six snapshots were extracted from a movie of 320 images that was acquired using a gradient echo MRE sequence every 1.5 s.

product between $\varphi_i(\vec{r},t)$ and the time-reversed field $\varphi_i(\vec{r}_0,-t)$ of a virtual point source located at $\vec{r}_0$ is computed:

$$\Psi_i^{TR}\left(\vec{r},t\right)=\phi_i\left(\vec{r}_0,-\tau\right)\overset{\otimes}{_t}\phi_i\left(\vec{r},\tau\right). \qquad [1]$$

Eq. **1** is widely used in seismology (14, 15) and known as correlation. Using a first signal analysis interpretation of Ψ_i^{TR}, it is quite straightforward to realize that its maximum, the autocorrelation, is reached on the virtual point source located on $\vec{r}=\vec{r}_0$ and for the zero lag time $t_0=0$ s. From this point $\vec{r}_0$, the spatial coherence slowly decreases, and it has a typical length that is proportional to the mean wavelength. Indeed, snapshots are acquired at a sampling time longer than the mean wave period. Therefore, they show independent wave patterns, which prevent the determination of the exact time course of the wave. Nevertheless, the existence of wave patterns implies that motion in one region is correlated with motion in its vicinity at a distance of a mean wavelength. This spatial extension is the key parameter to estimate the shear wavelength. It is close to what is known as the spectral autocorrelation method in seismology. A second physical time-reversal interpretation of correlation states that Ψ_i^{TR} is the field that would be observed if the sources responsible for the noise waves were able to be controlled and acting as a time-reversal mirror. The waves would, thus, backpropagate and reach the location of the virtual point source $\vec{r}_0$ at a special spatiotemporal refocusing time t_0. The energy concentration at t_0 defines a region around the virtual source $\vec{r}_0$ called the focal spot. This approach offers a simple and robust way to estimate the mean wavelength (Fig. 2*A*); indeed, the time-reversal focal spot reaches the diffraction limit that is known as the Rayleigh criterion (16, 17). The sampling rate under the Nyquist–Shannon limit prevents the computation of the time-reversal field as a function of time but leaves the spatiotemporal refocusing at time t_0 unaltered (18, 19). The extraction of the shear wavelength as spatial information from this latter time-reversal field $\Psi_i^{TR}(\vec{r},t_0)$ does not contradict the Nyquist–Shannon sampling theorem that addresses time information. However, the wave-frequency part of the time information is lost. A complete shear-wave speed estimation using this approach would, thus, need an independent measurement of frequency. The local wavelength estimation on the virtual point source located on $\vec{r}=\vec{r}_0$ is extracted from the focal spot along one axis *j* according to

$$\lambda_j\left(\vec{r}_0\right)\approx 2\pi\sqrt{\frac{\Psi_i^{TR}\left(\vec{r}_0,t_0\right)}{\xi_{ij}^{TR}\left(\vec{r}_0,t_0\right)}}, \qquad [2]$$

where ξ_{ij}^{TR} is the time-reversed strain field. The time reversed strain field follows from Eq. **1** by replacing the field ϕ_i by its gradient $\varepsilon_{ij}=\partial\varphi_i/\partial r_j$. The underlying diffuse field assumption is an isotropic random superposition of plane waves (20). It implies that $\varepsilon_{ij}\approx k_j\varphi_i$, with k_j as the wave number. Therefore, the time-reversal strain field becomes

$$\begin{aligned}\xi_{ij}^{TR}\left(\vec{r},t\right)&=\varepsilon_{ij}\left(\vec{r}_0,-\tau\right)\overset{\otimes}{_t}\varepsilon_{ij}\left(\vec{r},\tau\right)\\&\approx k_j\left(\vec{r}_0\right)\phi_i\left(\vec{r}_0,-\tau\right)\overset{\otimes}{_t}k_j\left(\vec{r}\right)\phi_i\left(\vec{r},\tau\right).\end{aligned} \qquad [3]$$

On the virtual point source at the zero lag time, the following equation is deduced:

$$\xi_{ij}^{TR}\left(\vec{r}_0,t_0\right)\approx k_j^2\left(\vec{r}_0\right)\Psi_i^{TR}\left(\vec{r}_0,t_0\right). \qquad [4]$$

The autocorrelation of the field gradient is, thus, equivalent to a curvature measurement, similar to the Laplacian computation

used in MRE reconstruction algorithms. It is now straightforward to deduce **2**. Although in theory, the wavelength can be estimated along three orthogonal directions j, it is limited in practice to the two dimensions of slices; a full 3D MRE sequence still needs to be tested. Moreover, in isotropic media, one direction only is sufficient. The brain anisotropy is ignored in this manuscript. Finally, **2** has been validated through simulations and experiments using ultrasounds (18).

The dimensions of the focal spot vary according to the local stiffness of the medium at the location $\vec{r}_0$ chosen for the virtual point source: a small focal spot in the soft inclusion, a medium one in the background, and a large one in the hard inclusion (Fig. 2*A*). The same logic holds for the focal spots in the two remaining inclusions (Fig. S1). As a consequence, by sequentially selecting each point of the field as a virtual source location $\vec{r}_0$, tomography of the wavelength is conducted in a processing time of 1 s. Compared with a T2-weighted sequence (Fig. 2*B*), the wavelength tomography shows good agreement on the location and the size of the four inclusions (Fig. 2*C*); a slight geometric distortion probably introduced by the effect of magnetic field inhomogeneity on the echo planar acquisition (EPI) is also visible. As expected, their growing stiffness is clearly apparent from left to right. When accounting for frequency-dependent motion-encoding gradient sensitivity, the central frequency of the vibrations measured within the phantom is ~80 Hz. At 80 Hz, the estimated shear wavelengths are 1.7, 2.9, 5.4, and 6.4 cm in each inclusion, respectively, and 3.6 cm in the background. Based on the relationship $\lambda = \sqrt{E/3\rho f_0^2}$ and Young's modulus E provided by the manufacturer, the expected shear wavelengths are 2.0, 2.7, 4.8, and 6.5 cm in each inclusion, respectively, and 3.6 cm in the background. As mentioned earlier, the correlation approach is efficient for a perfect diffuse field with the properties of equipartition (21). From this point of view, the multiple sources used in the experiment have two flaws. First, they are located on the surface, and second, they deliver synchronous vibrations. Although it is more difficult to experimentally implement, independent sources that are randomly distributed in the bulk represent the ideal situation of a perfect diffuse field for noise correlation techniques. Therefore, the imperfect source of this initial setup appears to be at the origin of the fluctuations in the wavelength tomography (Fig. 2*C* and Fig. S2). An inverse filter solution was proposed for seismic data (22). In this case, a spatial mean of $\Psi_i^{TR}(\vec{r}, t_0)$ can be simple and efficient. A typical 8-min MRE sequence only allows the acquisition of 320 frames of the elastic field, which are some 10–30% of those acquired in experiments conducted with ultrasounds (18). However, the correlation-based wavelength tomography clearly opens promising perspectives, and this approach was tested with the brains of two healthy adult volunteers.

Brain Experiments. The aim of passive elastography is to use natural shear-wave propagation in the human body. In the brain, the natural motion is caused by arterial pulsatility and cerebrospinal fluid exchange (23, 24). The MRE sequence presented in this section is the same as the one described for the phantom, except for the three following parameters: the voxel size of six slices is $4 \times 4 \times 4$ mm^3 to improve the signal to noise ratio (SNR), the total time of the in vivo experiments is 11 min, and three components of the displacements are acquired. The out-of-plane component only is investigated here. The first six 64×64-pixel snapshots shown in Fig. 3*A* show that the MRE sequence described in *Materials and Methods* can reveal the natural motion in the brain. The amplitudes are relatively small at only 5 μm, but the signal is clearly apparent. Because correlation computation is equivalent to an adaptive filter, the focal spot clearly emerges from the noise (Fig. 3*B*). The existence of these time-reversal focus spots is a convincing clue that natural motions in the brain are transported by shear waves. They are responsible for correlation decreasing down to negative values. The black −6-dB isolevel boundary lines more clearly illustrate the different sizes of the focal spots. With a mean of 10 cm, the wavelength estimations are within the expected range. Indeed, assuming that the motion is proportional to the intracranial pressure (25) and given the frequency-dependent sensitivity of the 50-Hz motion-encoding gradient used in our in vivo experiment, the central frequency of displacement (as encoded in the phase images) is expected to be ~1 Hz (13); 10% of energy is nonetheless present at a frequency of 15 Hz. It is expected that the wavelength estimation is dominated by the higher frequencies. Therefore, the shear-wave speed in the brain is around 1.5 m/s (26, 27). Therefore, the expected smaller wavelength ranges from 8 to 15 cm. In addition, longer wavelengths are observed on the periphery of the frontal

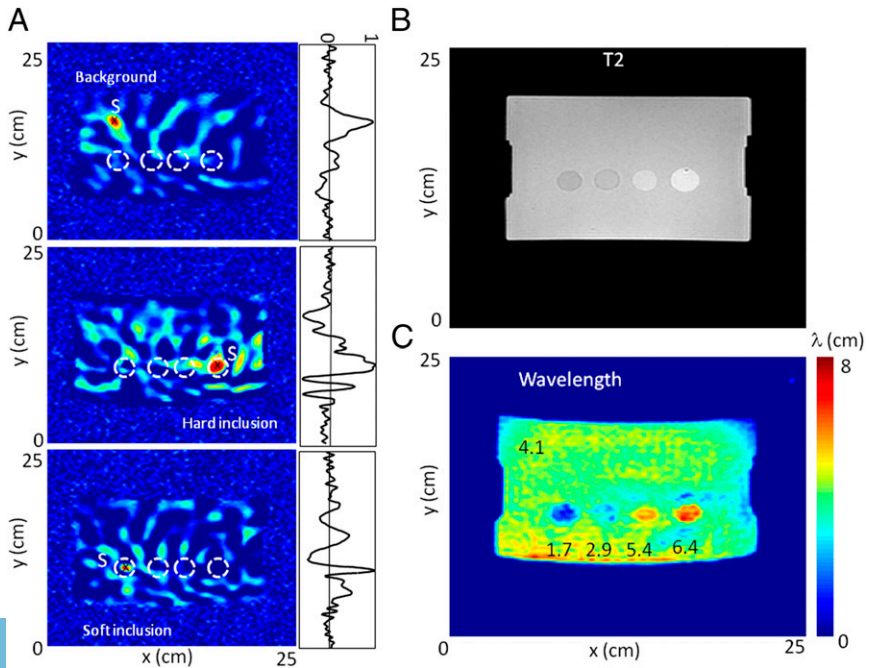

Fig. 2. Phantom correlation results. (*A*) Time-reversal focal spots for three different virtual source locations S in (*Top*) the phantom background (25 kPa), (*Middle*) the hard inclusion (80 kPa), and (*Bottom*) the soft inclusion (8 kPa). The virtual source S can be set arbitrarily to any location. (*B*) T2-weighted image of the phantom. (*C*) Shear-wavelength tomography. The four inclusions are clearly apparent, and their local wavelength estimations are proportional to the square root of their local elasticity.

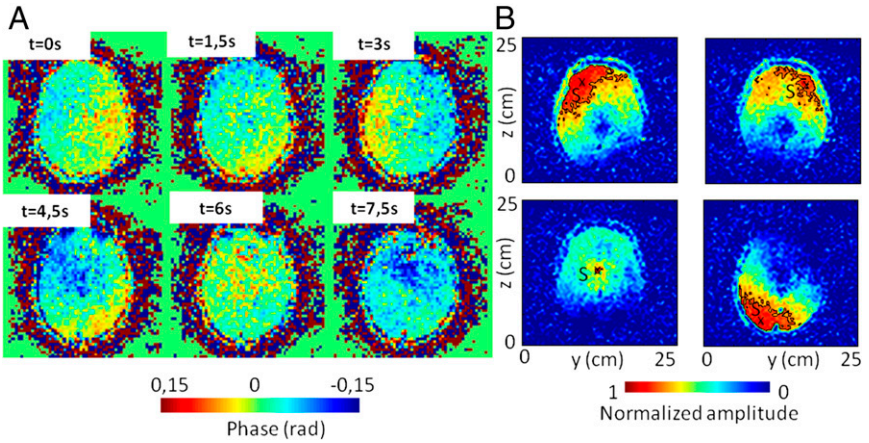

Fig. 3. In vivo brain results. (*A*) Phase representation of the displacement field. Six snapshots were extracted from a movie of 144 images. These in vivo measurements of brain motion were acquired with a gradient echo MRE sequence every 1.5 s. (*B*) Time-reversal focal spots in the brain for four different virtual source locations S. The isolevel black boundary lines stress the shear-wavelength variations.

and parietal lobes than in the center of the brain (Fig. 3*B*), which is clearly apparent on the shear-wavelength tomography reconstructions (Fig. 4). The anatomic details of T2 images are apparent on the shear-wavelength tomography, especially along the longitudinal fissure in the axial view (Fig. 4*A*). Finally, the longest wavelengths are visible in the posterior region of the brain (Fig. 4).

Discussion

The general results extracted from the first brain correlation reconstructions were verified on the same volunteer at a 1-mo interval as well as a second healthy volunteer (Figs. S3 and S4). Healthy volunteers were on their backs. The gravity-induced compression might enhance the local wavelength in the posterior brain. Additional studies of passive MRE are necessary to claim with confidence that these red posterior regions of the wavelength tomography reconstructions correspond to stiffer brain tissue (Fig. 4 and Fig. S4). Similarly, the apparent stiffer periphery region is not confirmed by MRE observations of the literature. Because it has to be a wave property effect, it is conjectured to be either a nonuniform frequency content of the shear-wave field or a change in the nature of the elastic wave with internal structure. At last, given that MRE includes three components of the field, that two orthogonal wavelength estimations are possible, and that the acquisition involves six different planes, we, therefore, end up with 36 possible tomography reconstructions. It is beyond the scope of this paper to offer detailed

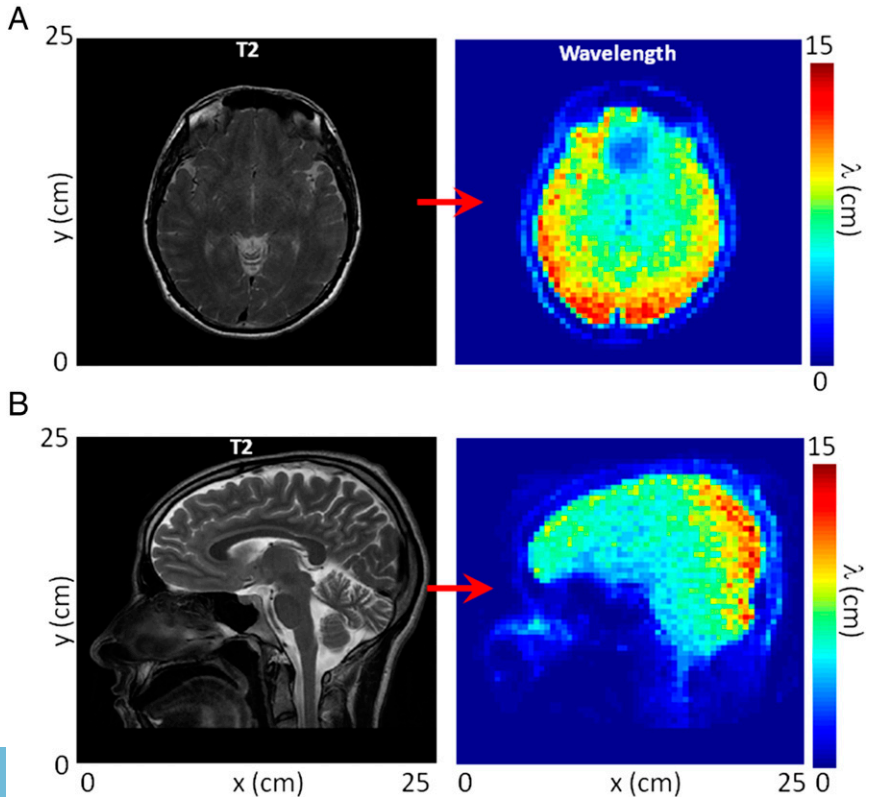

Fig. 4. In vivo brain passive MRE. (*A*) Axial view of (*Left*) the T2-weighted image and (*Right*) its corresponding shear-wavelength tomography. (*B*) Sagittal view of (*Left*) the T2-weighted image and (*Right*) its corresponding shear-wavelength tomography.

descriptions of each of these, although they are partly considered in Figs. S1, S2, S3, and S4. A promising possibility resides in the wave vector estimation that should partly reveal the brain anisotropy. In conclusion, the whole set of these experimental data brings us to the following statement: although natural tissue vibrations are often considered as disturbing noise, they nonetheless offer promising opportunities for medical imaging when correlation methods can be applied.

Materials and Methods

Instantaneous MRI snapshots are captured using a gradient echo single-shot echo planar imaging sequence (28) developed at the Mayo Clinic and installed on a 1.5-T system (General Electric). The displacement is encoded in the phase of the magnetic resonance signal using a 20-mT/m bipolar motion-encoding gradient applied over 10 ms (i.e., +20 mT/m over 5 ms immediately followed by −20 mT/m over 5 ms). The repetition and echo times are 1.5 s and 45 ms, respectively. In the phantom experiment, the field of view is $128 \times 128 \times 3$ mm, whereas it is $64 \times 64 \times 4$ mm in the brain experiment. The phantom is designed for elastography experiments by Computerized Imaging Reference Systems, Inc. The piezoelectric vibrator used in the phantom experiment is a PPA20M Cedrat Technologies. Institutional review board approval from Inserm was given and written informed consent was obtained from both volunteers.

ACKNOWLEDGMENTS. We acknowledge R. Ehman and K. Glaser from the Mayo Clinic for making the magnetic resonance elastography (MRE) sequences available.

1. Duvall TL, et al. (1993) Time-distance helioseismology. *Nature* 362(6419):430 (abstr).
2. Weaver RL, Lobkis OI (2001) Ultrasonics without a source: Thermal fluctuation correlations at MHz frequencies. *Phys Rev Lett* 87(13):134301.
3. Sabra KG, et al. (2007) Passive in vivo elastography from skeletal muscle noise. *Appl Phys Lett* 90(19):194101.
4. Lerosey G, de Rosny J, Tourin A, Fink M (2007) Focusing beyond the diffraction limit with far-field time reversal. *Science* 315(5815):1120–1122.
5. Sandrin L, Catheline S, Tanter M, Hennequin X, Fink M (1999) Time-resolved pulsed elastography with ultrafast ultrasonic imaging. *Ultrason Imaging* 21(4): 259–272.
6. Bercoff J, Tanter M, Fink M (2004) Supersonic shear imaging: A new technique for soft tissue elasticity mapping. *IEEE Trans Ultrason Ferroelectr Freq Control* 51(4): 396–409.
7. Nightingale K, Soo MS, Nightingale R, Trahey G (2002) Acoustic radiation force impulse imaging: In vivo demonstration of clinical feasibility. *Ultrasound Med Biol* 28(2):227–235.
8. Gallot T, et al. (2011) Passive elastography: Shear-wave tomography from physiological-noise correlation in soft tissues. *IEEE Trans Ultrason Ferroelectr Freq Control* 58(6):1122–1126.
9. Muthupillai R, et al. (1995) Magnetic resonance elastography by direct visualization of propagating acoustic strain waves. *Science* 269(5232):1854–1857.
10. Plewes DB, Betty I, Urchuk SN, Soutar I (1995) Visualizing tissue compliance with MR imaging. *J Magn Reson Imaging* 5(6):733–738.
11. Derode A, et al. (2003) How to estimate the Green's function of a heterogeneous medium between two passive sensors? Application to acoustic waves. *Appl Phys Lett* 83(15):3054 (abstr).
12. Fink M (1997) Time reversed acoustics. *Phys Today* 50(3):34 (abstr).
13. Weaver JB, et al. (2012) Brain mechanical property measurement using MRE with intrinsic activation. *Phys Med Biol* 57(22):7275–7287.
14. Campillo M, Paul A (2003) Long-range correlations in the diffuse seismic coda. *Science* 299(5606):547–549.
15. Snieder R, Wapenaar K, Wegler U (2007) Unified Green's function retrieval by cross-correlation; connection with energy principles. *Phys Rev E Stat Nonlin Soft Matter Phys* 75(3 Pt 2):036103.
16. de Rosny J, Fink M (2002) Overcoming the diffraction limit in wave physics using a time-reversal mirror and a novel acoustic sink. *Phys Rev Lett* 89(12):124301.
17. Catheline S, Benech N, Brum J, Negreira C (2008) Time reversal of elastic waves in soft solids. *Phys Rev Lett* 100(6):064301.
18. Catheline S, et al. (2013) Tomography from diffuse waves: Passive shear wave imaging using low frame rate scanners. *Appl Phys Lett* 103(1):014101 (abstr).
19. Benech N, Brum J, Catheline S, Gallot T, Negreira C (2013) Near-field effects in Green's function retrieval from cross-correlation of elastic fields: Experimental study with application to elastography. *J Acoust Soc Am* 133(5):2755–2766.
20. Weaver RL (1982) On diffuse waves in solid media. *J Acoust Soc Am* 71(6):1608 (abstr).
21. Roux P, Sabra KG, Kuperman WA, Roux A (2005) Ambient noise cross correlation in free space: Theoretical approach. *J Acoust Soc Am* 117(1):79–84.
22. Gallot T, Catheline S, Roux P, Campillo M (2012) A passive inverse filter for Green's function retrieval. *J Acoust Soc Am* 131(1):EL21–EL27.
23. McGarry MDJ, et al. (2015) Suitability of poroelastic and viscoelastic mechanical models for high and low frequency MR elastography. *Med Phys* 42(2):947–957.
24. Arani A, et al. (2015) Measuring the effects of aging and sex on regional brain stiffness with MR elastography in healthy older adults. *Neuroimage* 111:59–64.
25. Wagshul ME, Eide PK, Madsen JR (2011) The pulsating brain: A review of experimental and clinical studies of intracranial pulsatility. *Fluids Barriers CNS* 8(1):5.
26. Kruse SA, et al. (2008) Magnetic resonance elastography of the brain. *Neuroimage* 39(1):231–237.
27. Sack I, Beierbach B, Hamhaber U, Klatt D, Braun J (2008) Non-invasive measurement of brain viscoelasticity using magnetic resonance elastography. *NMR Biomed* 21(3):265–271.
28. Souchon R, et al. (2008) Transient MR elastography (t-MRE) using ultrasound radiation force: Theory, safety, and initial experiments in vitro. *Magn Reson Med* 60(4):871–881.